Iron at Earth's core conditions from first principles calculations

Dario Alfè
Department of Earth Sciences, and Department of Physics and Astronomy,
and London Centre for Nanotechnology, University College London,
Gower Street, London, WC1E 6BT, U.K

June 4, 2010

Abstract

Ab initio techniques, mainly based on the implementation of quantum mechanics known as density functional theory, and more recently quantum Monte Carlo, have now become widely used in the investigation of the high pressure and temperature properties of materials. These techniques have been proven reliable and accurate, and as such can be considered in many cases as complementary to experiments. Here I will describe some applications of ab-initio techniques to the properties of iron under Earth's core conditions. In particular, I will focus on the description of how to obtain high pressure and high temperature properties, as these are the relevant conditions of interests for the Earth's core. Low temperature properties of solids have often been studied using the quasi-harmonic approximation, which sometimes can retain high accuracy even at temperatures not too far from the melting temperature. However, for solids at high temperature and for liquids the quasi-harmonic approximation fails, and I will describe how using the molecular dynamics technique, coupled with ab-initio calculations and the thermodynamic integration scheme, it is possible to compute the high temperature thermodynamic properties of both solids and liquids. Examples of the application of these techniques will include the calculation of many thermodynamic properties of iron and its melting curve, which can be used to to improve our understanding of the temperature of the Earth's core.

Contents

1 Introduction

We start the discussion by recalling the structure of the Earth, which can be broadly described in terms of three main shells. The outermost is the crust, with a thickness of only a few tens of kilometers, mainly formed by silicates. Below the crust we find the mantle, which is customarily divided in an upper mantle and a lower mantle, separated by a transition zone. The mantle makes up most of the volume of the Earth, extending to a depth of 2891 km, almost half way towards the centre, and like the crust is also mainly formed by silicates, and in particular by $Mg(Fe)SiO_3$ with some significant fraction of Mg(Fe)O and SiO_2. Below the mantle we find the core, which is divided in an outer liquid core extending from 2891 to 5150 Km depths and an inner solid core below that, down to the centre of the Earth at 6346 Km depth. It is widely accepted that the core is mainly formed by iron, possibly with some 5 to 10 % of nickel, plus a fraction of unknown light impurities which reduce

the density by 2-3 % in the solid and 6-7 % in the liquid with respect to the density of pure iron under the same pressure-temperature conditions.

Studying the high pressure and temperature properties of core and mantle forming materials is of fundamental importance to the understanding of the formation and evolution of our planet. In particular, knowledge of the thermal structure of the Earth and the thermoelastic properties of Earth forming minerals will help us to interpret and hopefully predict the behaviour of the dynamical processes that occour inside our planet, including the generation of the Earth's magnetic field through the geodynamo, and the convective processes in the mantle which are ultimately responsible for plate tectonics, earthquakes and volcanic eruptions.

Since the core is mainly formed by iron, it is relevant to study its high temperature high pressure properties in details. Here we will address some of these properties using first principles techniques.

The development of theoretical methods based on the very basic laws of nature of quantum mechanics (developed more than 80 years ago), coupled with the recent staggering increase of computer power ($\sim$ at least 10,000-fold in the past 15 years), has made it possible to approach these problems from a theoretical-computational point of view. When high level first-principles methods are used, the results are often comparable in quality with experiments, sometimes even providing informations in regions of the pressure-temperature space unaccessible to experiments.

With the term *first-principles* we refer here to those calculations based of the very basic laws of nature, in which no empirical adjustable parameter is used. Only fundamental constants of physics are allowed. Specifically, the relevant basic law of physics are those describing the interactions between nuclei and electrons, i.e. those of quantum mechanics. In practice, approximations to exact quantum mechanics need to be introduced to provide tools that can be actually used, however, as long as these approximations do not involve the introduction of empirical parameters we will still regard those techniques as first-principles.

The exact quantum mechanical treatment of a system containing a large number of atoms is a formidable task. The starting point of nearly every quantum mechanical calculation available is the so called adiabatic approximation, which exploits the large difference of mass between the nuclei and the electrons. Since the electrons are much lighter, they move so much faster that on the time-scale of the nuclei movement the latter can be considered as fixed. Therefore one solves only the electronic problem in which the nuclei are fixed and act as an external potential for the electrons. The energy of the electrons plus the Coulomb repulsion of the nuclei is a function of the position of the nuclei, and can act as a potential energy for the nuclei. This can be mapped in configuration space to create a potential energy surface, which can later be used to study the motion of the nuclei. Alternatively, forces can be calculated as the derivatives of the potential energy with respect to the position of the nuclei, and these can be used to move the atoms around, relax the system, solve the Newton's equations of motion and perform molecular dynamics simulations, or calculate harmonic vibrational properties like phonons. The potential energy can also be differentiated with respect to the simulation cell parameters, which provides information on the stress tensor. The solution of the electronic problem also provides insights into the electronic structure of the system, which can be examined to study physical properties like bonding, charge distributions, magnetic densities, polarizabilities and so forth.

Most first-principles studies of the high pressure and temperature properties of Earth's forming materials are based on the implementation of quantum mechanics known as density functional theory(DFT). This is a technique that was introduced about 45 years ago by Hohenberg and Kohn (HK) [1], and Kohn and Sham (KS) [2] in an attempt to simplify the calculation of the ground state properties of materials (in fact, later shown to be useful also for finite temperature properties [3]). The basic HK idea was to substitute the cumbersome many-body wavefunction of a system containing N particles, which is a function of $3N$ variables, with the particle density, which is only a function of 3 variables. The price to pay for this enormous simplification is a modification of the basic equations of quantum mechanics with the introduction of new terms, one of which, called exchange-correlation (XC) energy, is unfortunately still unknown. However, KS proposed a simple form for the XC functional, known as the local density approximation (LDA) [2], that would prove later as the insight which has made DFT so successful and so widespread today. More sophisticated XC functional were developed in the following decades, and are still being developed today, making DFT an evolving technique with increasingly higher accuracy. One additional attractive feature of DFT is the favourable scaling of computational effort with the size of the system. Traditional DFT techniques scale as N^3, where N is the number of electrons in the system, but large effort is being put into so called $o(N)$ techniques, which for some materials already provide a scaling which is only directly proportional to the size of the system [4, 5].

The limitations in accuracy due to the current state of the art of density functional theory are expected to be progressively removed, either through the formulation of new exchange-correlation functionals, or with

the developments of alternative techniques. Among these dynamical mean field theory [6] and quantum Monte Carlo [7] (QMC) are probably the most promising on a time scale of 5 to 10 years. In fact, QMC techniques have recently been applied to iron at Earth's core conditions, and I will report results on the zero temperature iron equation of state and the iron melting temperature at 330 GPa.

In the next section I will introduce the main ideas to calculate zero temperature properties of materials, and I will report on some zero temperature properties or iron. In the following section I will move to the description of standard statistical mechanics tools for the calculation of free energies needed at high temperature. This will be done by separating the low temperature regime, where solids can be described within the quasi-harmonic approximation, from the high temperature regime, where the technique of thermodynamics integration is introduced to calculate free energies, both for solids and for liquids. As applications of these techniques, I will report on some high temperature high pressure properties of solid and liquid iron, including its melting curve at Earth's core conditions.

2 Static properties

2.1 Crystal structures and phase transitions

At zero temperature the main thermodynamic variable is the internal energy of the system E, or more generally at finite pressure p the enthalpy $H = E + pV$, where V is the volume of the system. The simplest possible first principles calculation one can do is the evaluation of the total energy of a system containing a certain number of atoms at fixed lattice sites. To find the most stable configuration of the atoms one simply minimises the total energy with respect to the atomic positions. This is usually done by evaluating forces, which are then used to move the atoms towards their equilibrium positions. For simple crystal structures this may not be necessary, as the positions may be constrained by symmetry. An example of this is solid iron in either its ambient conditions body-centred-cubic (bcc) crystal structure. As the pressure is increased the crystal structure of the material may change, and in fact in iron we find a transition from bcc to the hexagonal-close-packed (hcp) structure between 10 and 15 GPa [8]. The pressure at which the phase transformation occours is defined by the point where the enthalpies of the two crystal structures cross. These enthalpies can be computed using ab-initio techniques, by computing the energy E and the pressure p of the crystal as function of volume V, and then construct the enthalpy $H = E + pV$. By contrast with bcc, the hcp crystal structure has an additional degree of freedom, coming from the lack of a symmetry relating the hexagonal plane and the direction perpendicular to the plane. This additional degree of freedom, known as the c/a ratio, needs to be optimised for every volume V (we will return below on the issue of the optimal c/a for hcp iron at Earth's core conditions). Once this is done, an enthalpy curve can be constructed and compared with that obtained from the bcc structure. Calculations using DFT with the LDA or various generalised gradient approximations (GGA) have been performed, and it has been shown that in this particular case the LDA gives poor agreement with the experiments, even failing to predict the correct zero pressure crystal structure [9, 10, 11, 12, 13], while the GGA known as PW91 [14], for example, predicts the transition between 10 and 13 GPa [15], in good agreement with the experimental value which is in the range 10-15 GPa [8]. In Fig. 1 I show a comparison of the DFT-PW91 calculated equation of state with experiments. The calculations of Ref. [15] have been adapted to contain room temperature thermal expansion (see below), and agree very well with the experimental data [16, 17]. The figure also reports recent QMC calculations [18], which like the DFT-PW91 ones are in good agreement with the experiments.

2.2 Elastic constants

Most of what we know about the interior of our planet comes from seismology, and therefore from the elastic behaviour of the minerals inside the Earth. The theory of elasticity of crystals can be found in standard books [19]. Briefly, if a crystal is subjected to an infinitesimal stress $d\sigma_{ij}$, with i and j running through the three Cartesian directions in space, then it will deform according to the strain matrix $d\epsilon_{ij}$:

$$d\sigma_{ij} = \sum_{k,l} c_{ijkl} d\epsilon_{kl} \ . \tag{1}$$

The constant of proportionality between stress and strain, c_{ijkl} is a rank-4 tensor of elastic constants. With no loss of generality we can assume $d\sigma_{ij}$ and $d\epsilon_{ij}$ to be symmetric ($d\sigma_{ij} \neq d\sigma_{ji}$ would imply a non-zero torque

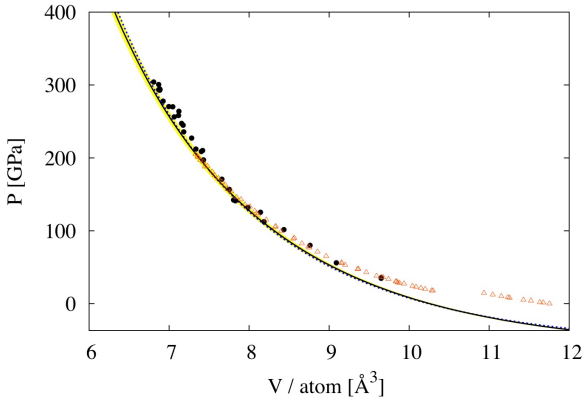

Figure 1: Pressure vs volume curve obtained from QMC calculations (solid line, with error band). DFT-PW91 results [15] (dotted line) and experimental data (circles [16] and open triangles [17]) are also reported for comparison. Room temperature thermal expansion has been added to the theoretical curves. Notice the discontinuity due to the hcp-bcc phase transition in the values provided by Dewaele *et al.* [17]. At low pressures, calculations and experiments differ because of the magnetism, which is not taken into account in the theoretical calculations. Reprinted from Ref. [18]. Copyright 1998 American Physical Society.

on the crystal, which would simply impose an angular acceleration and not a deformation), and therefore the elastic constant tensor is also symmetric. It is therefore possible to rewrite the rank-2 tensors $d\sigma_{ij}$ and $d\epsilon_{ij}$ as 6 components vectors, in the Voigt notation, with the index pairs 11, 22, 33, 23, 31, and 12 represented by the six symbols 1, 2, 3, 4, 5 and 6 respectively. In this notation, the stress-strain relation appears as:

$$d\sigma_i = \sum_j C_{ij} d\epsilon_j \ , \tag{2}$$

with i and j going from 1 to 6. Elastic constants are given as the coefficients C_{ij}. The matrix C_{ij} is symmetric, so that the maximum number of independent elastic constants of a crystal is 21. Because of crystal symmetries, the number of independent constants is usually much smaller. For example, in cubic crystals like bcc Fe there are only three elastic constants, in hcp Fe there are five.

Equation 2 provides the route to the calculation of the elastic properties of materials, and it can be applied both at zero and high temperatures. At zero temperature the components of stress tensor can be calculated as (minus) the partial derivative of the internal energy with respect to the components of the strain:

$$\sigma_{ij} = -\partial E / \partial \epsilon_{ij} | \epsilon, \tag{3}$$

Examples of zero temperature calculations of elastic constants include the DFT calculations of Stixrude and Cohen [20] on the hcp crystal structure of iron at Earth's inner core conditions, who suggested a possible mechanism based on the partial alignment of hcp crystallites to explain the seismic anisotropy of the Earth's inner core.

3 Finite temperature

The extension to finite temperature properties of materials may simply be obtained by substituting the internal energy E with the Helmholtz free energy F. The pressure p is obtained as (minus) the partial derivative of F with respect to volume, taken at constant temperature:

$$p = -\partial F / \partial V |_T. \tag{4}$$

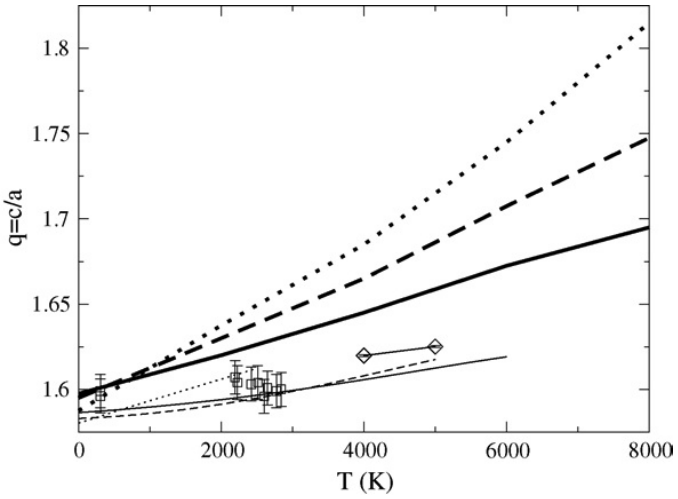

Figure 2: Calculated equilibrium c/a ratio in hcp iron as function of temperature for different volumes. For the work of Gannarelli et al. [24] (light curves) atomic volumes are 6.97 Å^3 (solid curve), 7.50 Å^3 (dashed curve) and 8.67 Å^3 (dotted curve). For the work of Steinle-Neumann et al [22] (heavy curves) volumes are 6.81 Å^3 (solid curve), 7.11 Å^3 (dashed curve) and 7.41 Å^3 (dotted curve). Also shown are the diffraction measurements due to Ma et al. [25] at 7.73 Å^3/atom (open squares with error bars and the molecular dynamics results of Gannarelli et al. [24] (open diamonds) at 6.97 Å^3. Reprinted from Ref. [24]. Copyright 2005 Elsevier.

If the system of interest is at sufficiently high temperature (above the Debye temperature), the nuclei can be treated as classical particles, and the expression of the Helmholtz free energy F for a system of N identical particles enclosed in a volume V, and in thermal equilibrium at temperature T is [21]:

$$F = -k_{\mathrm{B}}T \ln \left\{ \frac{1}{N!\Lambda^{3N}} \int_V d\mathbf{R}_1 \dots d\mathbf{R}_N \, e^{-\beta U(\mathbf{R}_1,\dots \mathbf{R}_N;T)} \right\}, \tag{5}$$

where $\Lambda = h/(2\pi M k_{\mathrm{B}}T)^{1/2}$ is the thermal wavelength, with M the mass of the particles, h the Plank's constant, $\beta = 1/k_{\mathrm{B}}T$, k_{B} is the Boltzmann constant, and $U(\mathbf{R}_1, \dots \mathbf{R}_N; T)$ the potential energy function, which depends on the positions of the N particles in the system, and possibly on temperature, in which case U is the electronic free energy.

The multidimensional integral extends over the total volume of the system V, and it is in general very difficult to calculate. In 2001 Steinle-Neumann et al. [22] modeled hcp iron using the *particle in a cell* technique, in which the potential energy experienced by any iron atom in the solid is approximated with an empirical potential fitted to first principle calculations, which coupled with the neglect of correlations between vibrations in different primitive cells makes it possible to integrate analytically Eq. 5. They calculated the free energy of the hcp solid as function of various strains applied to the cell at various temperatures, in the same spirit as described in the previous section, and obtained high temperature elastic constants. One of the main conclusions of their work was that at high temperature the elastic behaviour of iron is surprisingly different form the zero temperature behaviour, and in particular a large increase in the c/a parameter with temperature would result in a different prediction of partial alignment of crystals in the solid core from that inferred using zero temperature elastic constants [20]. However, subsequent calculations by Gannarelli et al. [23, 24] using the same method did not confirm the large increase of c/a in hcp iron predicted by Steinle-Neumann et al [22]. The two sets of results are displayed in Fig. 2, which also reports some recent experimental data [25], confirming the small increase of the c/a ratio with temperature predicted by Gannarelli et al. [24].

In the general case where the potential energy is not an easy quantity to compute one has to resort to different methods. For example, first principles high temperature elastic constants of iron at core conditions have been calculated by Vočadlo using molecular dynamics [26]. Here the deformations required in Equation 2 were imposed on the cell much in the same way as in the zero temperature case, but the resulting stresses were calculated as averages over molecular dynamics trajectories.

Using molecular dynamics simulations it is also possible to study the properties of liquids. For example, in a liquid the atoms are free to diffuse throughout the whole volume, and this behavior can be characterized

by diffusion coefficients D_α, where α runs over different species in the system. These D_α are straightforwardly related to the mean square displacement of the atoms through the Einstein relation [27]:

$$\frac{1}{N_\alpha}\langle\sum_{i=1}^{N_\alpha}|\mathbf{r}_{\alpha i}(t_0+t)-\mathbf{r}_{\alpha i}(t_0)|^2\rangle \rightarrow 6D_\alpha t, \quad \text{as} \quad t\rightarrow\infty, \tag{6}$$

where $\mathbf{r}_{i\alpha}(t)$ is the vector position at time t of the i-th atom of species α, N_α is the number of atoms of species α in the cell, and $\langle\rangle$ means time average over t_0. The diffusion coefficient can also be used to obtain a rough estimate of the viscosity η of the liquid, by using the relation between the two stated by the Stokes-Einstein relation:

$$D\eta = \frac{k_B T}{2\pi a}. \tag{7}$$

This technique was used by de Wijs et al. [28] to estimate the viscosity of liquid iron at Earth's core conditions. The Stokes-Einstein relation in Eq. 7 is exact for the Brownian motion of a macroscopic particle of diameter a in a liquid of viscosity η. The relation is only approximate when applied to atoms; however, if a is chosen to be the nearest neighbors distance of the atoms in the solid, Eq. 7 provide results which agree within 40% for a wide range of liquid metals. To calculate the viscosity rigorously, it is possible to use the Green-Kubo relation:

$$\eta = \frac{V}{k_B T}\int_0^\infty dt\langle\sigma_{xy}(t)\sigma_{xy}(0)\rangle, \tag{8}$$

where σ_{xy} is the off-diagonal component of the stress tensor $\sigma_{\alpha\beta}$ (α and β are Cartesian components). This relation was used in the context of first principles calculations for the first time by Alfè and Gillan [29], who first calculated the viscosity of liquid aluminium at ambient pressure and a temperature of 1000 K, showing that the method provided results in good agreement with the experiments, and then applied the method to the calculation of the viscosity of a liquid mixture of iron and sulphur under Earth core conditions. In Fig. 3 I show the integral in Eq. 8 calculated from 0 to time t for this iron sulphur liquid mixture. In principle, this has to be computed from zero to infinity, as stated in Eq. 8, however, in this particular case there is nothing to be gained by extending the integral beyond about 0.2 ps, after which the integrand has decayed to zero and it is dominated by statistical noise. The figure also shows the computed statistical error on the integral, and from this it was possible to infer the value for the viscosity $\eta = 9 \pm 2$ mPa s, in good agreement with that obtained from the diffusion coefficient via the Einstein relation 7, calculated to be $\eta \sim 13$ mPa s in a previous paper [30].

In the next two section I will now introduce the standard techniques to obtain free energies at finite temperature from first principles calculations.

3.1 The Helmholtz free energy: low temperature and the quasi-harmonic approximation

For a solid at low temperature, the Helmholtz free energy F can be easily accessed by treating the system in the quasi-harmonic approximation. This is done by expanding the potential (free) energy function U around the equilibrium positions of the nuclei. The first term of the expansion is simply the energy of the system calculated with the ions in their equilibrium positions, $E_{\rm perf}(V,T)$ (this is a free energy at finite temperature, and therefore depends both on V and T). If the crystal is in its minimum energy configuration the linear term of the expansion is zero, and by neglecting terms of order three and above in the atomic displacements we have that the quasi-harmonic potential is:

$$U_{\rm harm} = E_{\rm perf} + \frac{1}{2}\sum_{ls\alpha,l't\beta}\Phi_{ls\alpha,l't\beta}u_{ls\alpha}u_{l't\beta}, \tag{9}$$

where $\mathbf{u}_{ls}$ denotes the displacement of atom s in unit cell l, α and β are Cartesian components, and $\Phi_{ls\alpha,l't\beta}$ is the force-constant matrix, given by the double derivative $\partial^2 U/\partial u_{ls\alpha}\partial u_{l't\beta}$ evaluated with all atoms at their equilibrium positions. This force constant matrix gives the relation between the forces $\mathbf{F}_{ls}$ and the displacements $\mathbf{u_{l't}}$, as can be seen by differentiating Eq. 9 and ignoring the higher-order an-harmonic terms:

$$F_{ls\alpha} = -\partial U/\partial u_{ls\alpha} = -\sum_{l't\beta}\Phi_{ls\alpha,l't\beta}u_{l't\beta}\ . \tag{10}$$

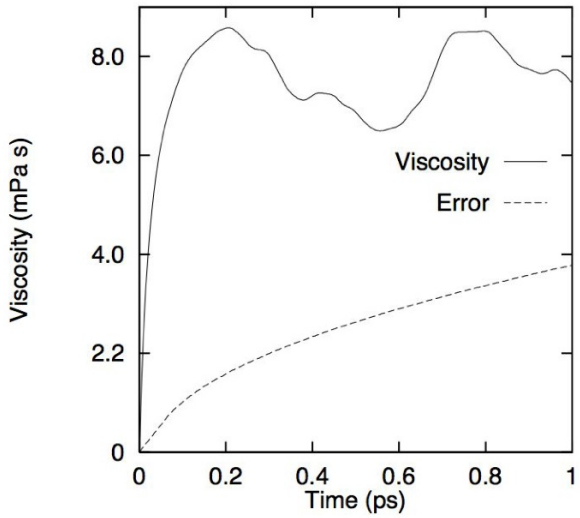

Figure 3: Viscosity integral of the average stress autocorrelation function and its statistical error as a function of time for liquid Fe-S under Earth's core conditions. Reprinted from Ref. [29]. Copyright 1998 American Physical Society

Within the quasi-harmonic approximation, the potential energy function $U_{\rm harm}$ completely determines the physical properties of the system, and in particular the free energy, which takes the form:

$$F(V,T) = E_{\rm perf}(V,T) + F_{\rm harm}(V,T), \tag{11}$$

where the quasi-harmonic component of the free energy is:

$$F_{\rm harm} = k_{\rm B}T \sum_n \ln(2\sinh(\hbar\omega_n/2k_{\rm B}T)) \ , \tag{12}$$

with ω_n the frequency of the nth vibrational mode of the crystal. In a periodic crystal, the vibrational modes can be characterised by a wave-vector $\mathbf{k}$, and for each such wave-vector there are three vibrational modes for every atom in the primitive cell. If the frequency of the sth mode at wave-vector $\mathbf{k}$ is denoted by $\omega_{\mathbf{k}s}$, then the vibrational free energy is:

$$F_{\rm harm} = k_{\rm B}T \sum_{\mathbf{k}s} \ln(2\sinh(\hbar\omega_{\mathbf{k}s}/2k_{\rm B}T)). \tag{13}$$

The vibrational frequencies $\omega_{\mathbf{k}s}$ can be calculated from first principles, for example using the small displacement method [31].

As an example of first principles calculations of phonon frequencies using the small displacement method I show in Fig. 4 the phonon dispersion relations for bcc iron under ambient conditions, compared with experimental data [32]. We see that the agreement between theory and experiments is very good almost everywhere in the Brillouin zone, with discrepancies being at worst $\sim 3\%$.

Phonons can also be calculated at high pressure, and as an illustration of this in Fig. 5 I show a comparison between DFT-PW91 calculations and nuclear resonant inelastic x-ray scattering (NRIXS) [33, 34] experiments, of phonon density of states of bcc and hcp iron from zero to 153 GPa [35]. The agreement between theory and experiments is good in the whole pressure region, being slightly better at high pressure.

Once the quasi-harmonic free energy is known, all the thermodynamical properties of the system can be calculated. In particular, the pressure is given by:

$$p = -\partial F/\partial V|_T = -\partial E_{\rm perf}/\partial V|_T - \partial F_{\rm harm}/\partial V|_T. \tag{14}$$

The last term in the equation above is the ionic component of the thermal pressure, and it is different from zero because the vibrational frequencies $\omega_{\mathbf{k}s}$ depend on the volume of the crystal. In fact, it is easy to see from Eq. 13

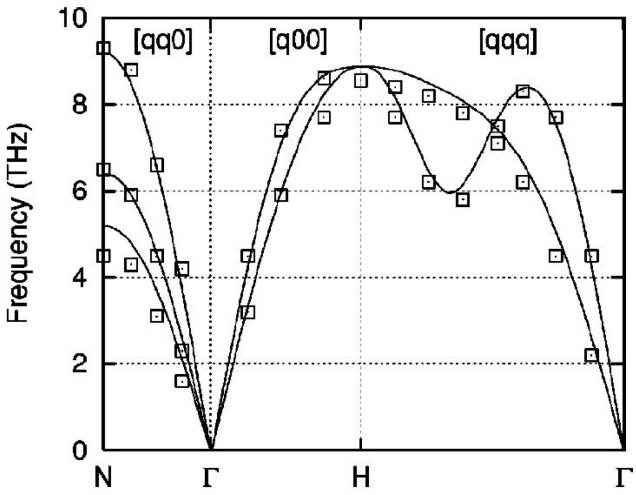

Figure 4: Phonon dispersion relations of ferromagnetic b.c.c. Fe. Lines and open squares show first-principles theory [15] and experiment respectively [32]. Reproduced from Ref. [15]. Copyright 2000 American Physical Society.

that even at zero temperature there is a finite contribution to the quasi-harmonic free energy, given by:

$$F_{\mathrm{harm}}(V,0) = \sum_{\mathbf{k}s} \frac{\hbar\omega_{\mathbf{k}s}}{2}. \tag{15}$$

This zero point energy contribution to the harmonic free energy is also responsible for a contribution to the pressure. Since usually the vibrational frequencies $\omega_{\mathbf{k}s}$ increase with decreasing volume, these contributions are positive, and are responsible for the phenomenon of thermal expansion in solids.

The dependence of $E_{\mathrm{perf}}(V,T)$ on T also means that there is an electronic contribution to the thermal pressure, which is also positive, and in some cases (i.e. iron at Earth's core conditions) can be a significant fraction of the thermal pressure, and a non-negligible fraction of the total pressure [36].

3.2 The Helmholtz free energy: high temperature and thermodynamic integration

At high temperature an-harmonic effects in solids may start to play an important role, and the quasi-harmonic approximation may not be accurate enough. Moreover, if the system of interest is a liquid, the quasi-harmonic approximation is of no use. In this section I shall describe a method to calculate the free energy of solids and liquid in the high temperature limit, provided that the temperature is high enough that the quantum nature of the nuclei can be neglected. If this is the case, the Helmholtz free energy F is defined as in Eq. 5.

Performing the integral in Eq. 5 to calculate F is extremely difficult if the potential energy is not a simple function of the ionic positions. However, it is less difficult to calculate changes in F as some specific variables are changed in the system. For example, we have seen that by taking the derivative of F in Eq. 5 with respect to volume at constant T we obtain (minus) the pressure. Therefore, the difference of F between two volumes can be obtained by integrating the pressure p, which can be calculated using a molecular dynamics simulation. Similarly, by integrating the internal energy E one obtains differences in F/T.

It is equally possible to calculate differences in free energy between two systems having the same number of atoms N, the same volume V, but two different potential energy functions U_0 and U_1. This can be done by introducing an intermediate potential energy function U_λ such that for $\lambda = 0; U_\lambda = U_0$, and for $\lambda = 1; U_\lambda = U_1$, and such that for any value of $0 < \lambda < 1, U_\lambda$ is a continuous and differentiable function of λ. For example, a convenient form is:

$$U_\lambda = (1 - f(\lambda))U_0 + f(\lambda)U, \tag{16}$$

where $f(\lambda)$ is an arbitrary continuous and differentiable function of λ in the interval $0 \leq \lambda \leq 1$, with the property

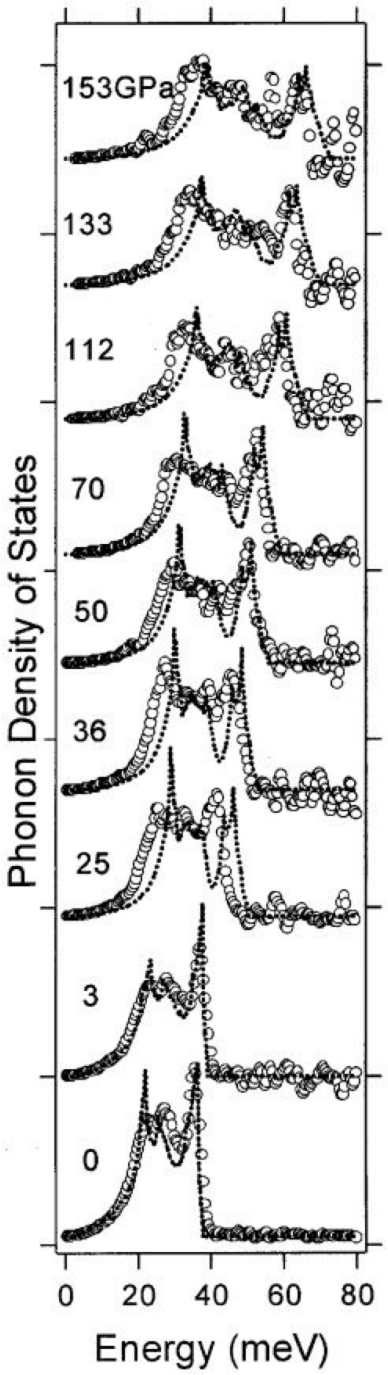

Figure 5: Phonon density of states of b.c.c Fe (pressure $p = 0$ and 3 GPa) and h.c.p. Fe (p from 25 to 153 GPa). Dotted curves and open circles show first-principles theory and experiment respectively. Reproduced from Ref. [35]. Copyright 2001 American Association for the Advancement of Science.

$f(0) = 0$ and $f(1) = 1$. According to Eq 5, the Helmholtz free energy of this intermediate system is:

$$F_\lambda = -k_\mathrm{B}T \ln \left\{ \frac{1}{N!\Lambda^{3N}} \int_V d\mathbf{R}_1 \dots d\mathbf{R}_N \, e^{-\beta U_\lambda(\mathbf{R}_1,\dots\mathbf{R}_N;T)} \right\}. \tag{17}$$

Differentiating this with respect to λ gives:

$$\frac{dF_\lambda}{d\lambda} = \frac{\int_V d\mathbf{R}_1 \dots d\mathbf{R}_N e^{-\beta U_\lambda(\mathbf{R}_1,\dots\mathbf{R}_N;T)} (\frac{\partial U_\lambda}{\partial \lambda})}{\int_V d\mathbf{R}_1 \dots d\mathbf{R}_N e^{-\beta U_\lambda(\mathbf{R}_1,\dots\mathbf{R}_N;T)}} = \left\langle \frac{\partial U_\lambda}{\partial \lambda} \right\rangle_\lambda, \tag{18}$$

and therefore by integrating dF_λ/d_λ one obtains:

$$\Delta F = F_1 - F_0 = \int_0^1 d\lambda \left\langle \frac{\partial U_\lambda}{\partial \lambda} \right\rangle_\lambda. \tag{19}$$

This also represents the reversible work done on the system as the potential energy function is switched from U_0 to U_1. In most cases a suitable choice for the function that mixes U_0 and U_1 is simply $f(\lambda) = \lambda$, and the thermodynamic formula 19 takes the simple form:

$$\Delta F = F_1 - F_0 = \int_0^1 d\lambda \left\langle U_1 - U_0 \right\rangle_\lambda. \tag{20}$$

This way to calculate free energy differences between two systems is called thermodynamic integration [21]. The usefulness of the thermodynamic integration formula expressed in Eq. 19 becomes clear when one identifies U_1 with the DFT potential (free) energy function, and with U_0 some classical model potential for which the free energy is easily calculated, to be taken as a reference system. Then Eq. 19 can be used to calculate the DFT free energy of the system by evaluating the integrand $\langle U_1 - U_0 \rangle_\lambda$ using FPMD simulations at a sufficiently large number of values of λ and calculating the integral numerically. Alternatively, one can adopt the dynamical method described by Watanabe and Reinhardt [37]. In this approach the parameter λ depends on time, and is slowly (adiabatically) switched from 0 to 1 during a single simulation. The switching rate has to be slow enough so that the system remains in thermodynamic equilibrium, and adiabatically transforms from the reference to the ab-initio system. The change in free energy is then given by:

$$\Delta F = \int_0^{T_\mathrm{sim}} dt \frac{d\lambda}{dt} \left(U_1 - U_0 \right), \tag{21}$$

where T_sim is the total simulation time, $\lambda(t)$ is an arbitrary function of t with the property of being continuous and differentiable for $0 \leq t \leq 1$, $\lambda(0) = 0$ and $\lambda(T_\mathrm{sim}) = 1$.

Thermodynamic integration can be used to calculate the free energies of both solids and liquids. It is clear from Eq. 19 that the choice of the reference system is almost completely irrelevant (of course, the stability of the system cannot change as λ is switched from 0 to 1), provided that ΔF can be calculated in practice. So, if the goal is to obtain ab-initio free energies, it is essential to minimise the amount of ab-initio work in order to make the calculations feasible. This is achieved by requiring that: *i*) the integrand in Eq. 19 is a smooth function of λ, *ii*) the thermal averages $\langle U_1 - U_0 \rangle_\lambda$ can be computed within the required accuracy on the time-scales accessible to FPMD and *iii*) the convergence of ΔF as function of the number of atoms N in the system is again achieved with N accessible to first-principles calculations. All points *i*),*ii*), and *iii*) could obviously be satisfied by a perfect reference system, i.e. a system which differed from the ab-initio system only by an arbitrary constant. In this trivial case the integrand Eq. 19 would be a constant, and thermal averages could be calculated on just one configuration and with cells containing an arbitrary small number of atoms. The next thing close to a constant is a slowly varying object, and this therefore provides the recipe for the choice of a good reference system, which has to be constructed in such a way that the fluctuations in $U_1 - U_0$ are as small as possible. If this is the case, thermal averages of $U_1 - U_0$ are readily calculated on short simulations. Moreover, $\langle U_1 - U_0 \rangle_\lambda$ is a smooth function of λ, so a very limited number of simulations for different values of λ are needed and, finally, convergence of $\langle U_1 - U_0 \rangle_\lambda$ with respect to the size of the system is also quick. In fact, if the fluctuations in $U_1 - U_0$ are small

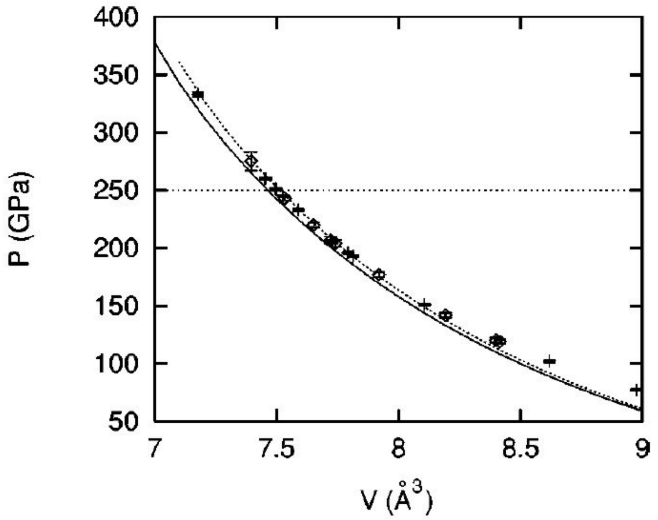

Figure 6: Experimental and first-principles Hugoniot pressure p of Fe as a function of atomic volume V. Symbols show the measurements of Brown and McQueen [40]. Solid curve is first-principles pressure obtained when calculated equilibrium volume of b.c.c. Fe is used in the Hugoniot-Rankine equation; dotted curve is the same, but with experimental equilibrium volume of b.c.c. Fe. The comparison is meaningful only up to a pressure of *ca.* 250 GPa (horizontal dotted line), at which point the experiments indicate melting. Reprinted from Ref. [39]. Copyright 2002 American Physical Society.

enough, one can simply write $F_1 - F_0 \simeq \langle U_1 - U_0 \rangle_0$, with the average taken in the reference system ensemble. If this is not good enough, the next approximation is readily shown to be:

$$F_1 - F_0 \simeq \langle U_1 - U_0 \rangle_0 - \frac{1}{2k_{\rm B}T} \left\langle [U_1 - U_0 - \langle U_1 - U_0 \rangle_0]^2 \right\rangle_0 . \tag{22}$$

This form is particularly convenient since one only needs to sample the phase space with the reference system, and perform a number of ab-initio calculations on statistically independent configurations extracted from a long classical simulation.

Once the Helmholtz free energy of the system is known, it can be used to derive its thermodynamical properties. For example, it is possible to calculate properties on the so-called Hugoniot line, and compare the results with those obtained in shock-wave experiments. The data that emerge most directly from shock experiments consist of a relation between the pressure $p_{\rm H}$ and the molar volume $V_{\rm H}$ on the Hugoniot line, which is the set of thermodynamic states given by the Rankine-Hugoniot formula [38]:

$$\frac{1}{2} p_{\rm H} (V_0 - V_{\rm H}) = E_{\rm H} - E_0 \ , \tag{23}$$

where $E_{\rm H}$ is the molar internal energy behind the shock front, and E_0 and V_0 are the molar internal energy and volume in the zero-pressure state ahead of the front. These experiments are particularly useful in identifying the melting transition. This is done by monitoring the speed of sound, which shows discontinuities at two characteristic pressures p_s and p_l, which are the points where the solid and liquid Hugoniots meet the melting curve. Below p_s, the material behind the shock front is entirely solid, while above p_l it is entirely liquid; between p_s and p_l, the material is a two-phase mixture. To illustrate an example of the quality of the DFT-PW91 predictions of the Hugoniot line I show in Fig. 6 the calculations of the $p(V)$ relation on the Hugoniot [39] for solid and liquid iron, compared with the experimental data obtained by Brown and McQueen [40]. We can see that the agreement between the theory and experiments is extremely good. The two theoretical curves come from raw and free energy corrected calculations (see below). In Fig. 7 I show a comparison of the calculated speed of sounds of the liquid with those obtained in the shock experiments. Again, the agreement between the two sets of data is extremely good.

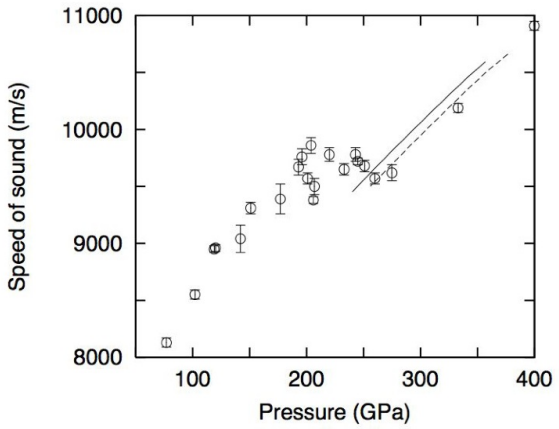

Figure 7: Longitudinal speed of sound on the Hugoniot. Circles: experimental values from Ref. [40]; continuous and dashed curves: ab initio values from Ref. [39] without and with free-energy correction (see text). Reprinted from Ref. [39]. Copyright 2002 American Physical Society.

3.3 Melting

Once the free energies of solid and liquid are known, it is possible to calculate also melting properties, including the whole melting curve of iron under Earth's core conditions [36, 39, 41, 42]. It was found that a simple sum of inverse power pair-potentials of the form $U_{\rm IP}(r) = B/r^{\alpha}$, where r is the distance between two ions and B and α are two adjustable parameters, did an excellent job in describing the energetics of the liquid and the high temperature solid, provided B and α were appropriately adjusted. As mentioned in the previous section, an additional crucial advantage of having a good reference system is that convergence of $F_1 - F_0$ with respect to the size of the system is very rapid, and in fact for both solid and liquid iron it was found that already with 64-atom systems $F_1 - F_0$ was converged to within better than 10 meV/atom, which in turns implied melting temperature converged to better than 100 K with respect to this single technical point. The best estimate for the melting point at the inner-outer core boundary pressure of 330 GPa was $T_m = 6350 \pm 300$ K [39], where the error quoted is the result of the combined statistical errors in the free energies of solid and liquid. Systematic errors due to the approximations of DFT are more difficult to estimate. Some empirical attempts at correcting the DFT-PW91 free energies were based on the differences between the DFT-PW91 zero temperature pressure-volume equation of state and the experimental data, resulting in the free energy corrected results reported in Figs. 6,7. Very recently, we re-addressed this problem going beyond approximated DFT, using quantum Monte Carlo techniques (see below).

At the present state of knowledge, the experimental understanding of the melting point of Fe under this conditions is still scarce, as experiments based on diamond-anvil cells (DAC) cannot reach these pressures. Moreover, even in the region of the phase space where DAC experiments are possible there is still considerable disagreement between different groups [25, 43, 44], and between DAC and shock-wave experiments [40, 45].

On the theoretical side, we mention also the work of Laio et al. [46] and Belonoshko et al. [47], who performed DFT based simulations to calculate the melting curve of Fe under Earth's core conditions, although their approach was rather different from ours [36, 39, 41, 42]. Instead of calculating free energies, Laio et al. [46] and Belonoshko et al. [47] fitted a classical model potential to their first principles calculations, and then used the classical potential to compute the melting curve. To do so, they used the coexistence method, in which solid and liquid are simulated in contact in a box. This method is an alternative route to the calculation of melting curves, and therefore equivalent to the free energy approach. However, Laio et al. and Belonoshko et al. found that at the pressure of 330 GPa iron melted at 5400 and 7000 K respectively. The reason of these large differences, and the difference with our value 6350 K, are due to the quality of the classical potentials employed, and in particular to the free energy differences between these classical potentials and the DFT system. This was later investigated by us [48], and it was shown that it is possible to assess the differences in free energies between the classical potential and the DFT one, and correct for it. In particular, it was shown that at a fixed pressure p, a first approximation

of the difference T' in the melting temperature between the classical potential and the ab-initio system is given by:

$$T' = \Delta G^{ls}\left(T_{\rm mod}\right)/S^{ls}_{\rm mod}, \tag{24}$$

where $S^{ls}_{\rm mod}$ is the entropy of fusion of the model potential, $T_{\rm mod}$ its melting temperature, and $\Delta G^{ls} = (G^l_{ab} - G^l_{mod}) - (G^s_{ab} - G^s_{mod})$, where G is the Gibbs free energy, the subscripts *ab* and *mod* indicate the ab-initio and the model system respectively, and the superscripts l and s indicate liquid and solid respectively. These differences of Gibbs free energies can be calculated using thermodynamic integration, which if the model potential is not too different fro the ab-initio one can be calculated using the perturbative approach outlined in Eq. 22 above. The relation between ΔG, evaluated at constant p, and ΔF, calculated at constant V, is readily shown to be:

$$\Delta G = \Delta F - \frac{1}{2} V \kappa_T \Delta p^2 + o(\Delta p^3), \tag{25}$$

where κ_T is the isothermal compressibility and Δp is the change of pressure when $U_{\rm mod}$ is replaced by $U_{\rm ab}$ at constant V and T. Once this corrections were applied, the results of Belonoshko et al. [47] came in perfect agreement with ours [39].

The coexistence method mentioned above is an alternative route to the calculation of melting properties, and as such delivers the same results if applied consistently. For its very nature, the method is intrinsically very expensive, because it requires simulations on systems containing large number of atoms, typically many hundreds or even thousands. For this reason, until very recently it had been only applied to calculations employing classical potentials. However, it has been recently shown that the method can in fact be applied also in the context of first principles calculations, and indeed it has been applied to the calculation of the melting temperature of iron at ICB pressure, with a result of 6390 ± 100 K [49]. The close agreement between the results obtained with the first principles coexistence and the first principles free energies support each other and confirm that the DFT melting temperature of iron at 330 GPa is in the region of 6350 K.

Recently, Sola and Alfè [50] re-addressed the problem using the quantum Monte Carlo technique. They performed thermodynamic integration between DFT and QMC exploiting Eq. 22. This was done by performing long DFT molecular dynamics simulations (using the VASP code [51]), and then calculating QMC (using the CASINO code [52]) and DFT energies on a selection of statistically independent configurations, which showed that fluctuations in energy differences between QMC and DFT are small and Eq. 22 can be used reliably (see Fig. 8). Then used Eq. 24 to compute a melting temperature correction of 550 ± 250 K. This correction is small, but maybe not completely negligible in terms of geophysical implications, which I will not discuss here. These results are all displayed in Fig. 9, together with a number of experimental data.

I would like to conclude by pointing out that QMC techniques are fairly easy to parallelise, and have already be shown to scale well on tens of thousands processors. These QMC techniques are 3 or 4 order of magnitudes more expensive than conventional DFT based techniques, however, because of their favorable scaling properties, they are likely to be able to exploit very effectively the computers of the future, and in a decade or two might reach the standards of utilisations that DFT techniques have today.

References

[1] Hohenberg P, Kohn W (1964) Inhomogeneous electron gas. Phys Rev 136:B864-B871

[2] Kohn W, Sham L (1965) Self-consistent equations including exchange and correlation effects. Phys Rev 140:A1133-A1138

[3] Mermin ND (1965) Thermal properties of the inhomogeneous electron gas. Phys Rev 137:A1441-A1443

[4] Bowler DR, Miyazaki T, Gillan MJ (2002) Recent progress in linear scaling ab initio electronic structure techniques. J Phys Condens Matter 14:2781-2798

[5] Soler JM, Artacho E, Gale JD, Garcia A, Junquera J, Ordejon P, Sanchez-Portal D (2002) The SIESTA method for ab initio order-N materials simulation. J Phys Condens Matter 14:2745-2779

[6] Savrasov PY, Kotliar G (2003) Linear response calculations of lattice dynamics in strongly correlated systems. Phys Rev 90:L056401 1-4

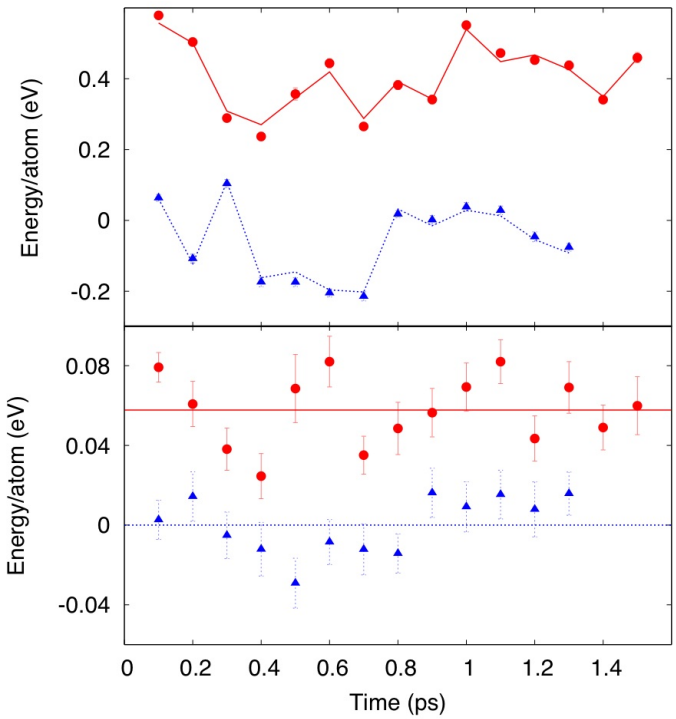

Figure 8: Top panel: QMC energies corresponding to configurations representative of solid (blue triangles) and liquid (red dots) iron, generated with DFT molecular dynamics on 64-atom systems. Red solid line and blue dashed line connect DFT energies calculated on the same set of configurations. An offset is added to the energies so that the average value of the QMC and DFT energies is the same, separately in the solid and the liquid. Bottom panel: QMC - DFT energy differences on the same configurations. The average QMC - DFT energy difference for the solid is subtracted from all points. Lines represent the average of the energy differences between QMC and DFT in the solid (line at zero energy) and the liquid. Reprinted from Ref. [50]. Copyright 2009 American Physical Society.

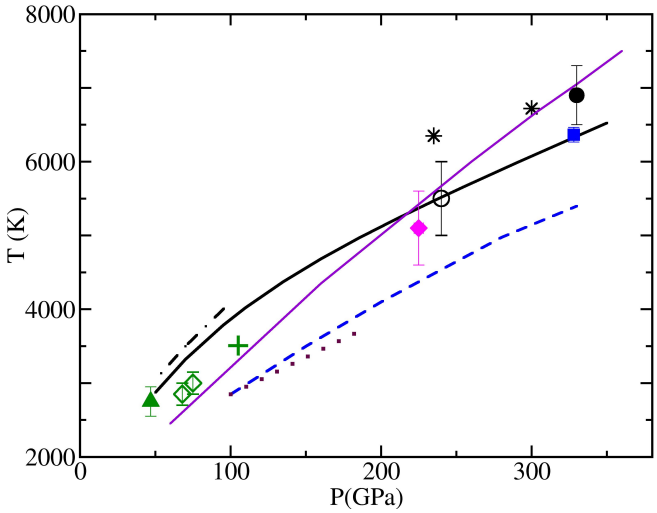

Figure 9: Comparison of melting temperatures (T) of Fe as function of pressure (P) from present calculations with experiments and other *ab initio* results. Black filled circle: present DMC results; blue filled square: melting point from DFT coexistence [49]; solid black line: melting curve from DFT free energies [39]; dashed blue curve: theoretical results from Ref. [46]; light purple solid curve: theoretical results from Ref. [47]; black chained and maroon dotted curves: DAC measurements of Refs. [54] and [43]; green open diamonds: DAC measurements of Ref. [44]; green plus: DAC measurement of Ref. [25]; green filled triangle: DAC measurement of Ref. [55]; black stars, black open circle and pink filled diamond: shock experiments of Refs. [53], [40] and [45]. Error bars are those quoted in original references. Reprinted from Ref. [50]. Copyright 2009 American Physical Society.

[7] Foulkes WMC, Mitaš L, Needs RJ, Rajagopal G (2001) Quantum Monte Carlo simulations of solids. Rev Mod Phys 73:33-83

[8] Jephcoat AP, Mao HK, Bell PM (1986) Static compression of iron to 78 GPa with rare gas solids as pressure-transmitting media. J Geophys Res 91:4677-4684

[9] Cho JH, Scheffler M (1996) Ab initio pseudopotential study of Fe, Co, and Ni employing the spin-polarized LAPW approach. Phys Rev 53:B10685-B10689

[10] Zhu J, Wang XW, Louie SG (1992) First-principles pseudopotential calculations of magnetic iron. Phys Rev 45:B8887-B8893

[11] Leung TC, Chan CT, Harmon BN (1991) Ground-state properties of Fe, Co, Ni, and their monoxides: results of the generalized gradient approximation. Phys Rev 44:B2923-B2927

[12] Körling M, Häglund J (1992) Cohesive and electronic properties of transition metals: the generalized gradient approximation. Phys Rev 45:B13293-B13297

[13] Singh DJ, Pickett WE, Krakauer H (1991) Gradient-corrected density functionals: full-potential calculations for iron. Phys Rev 43: B11628-B11634

[14] Wang Y, Perdew JP (1991) Correlation hole of the spin-polarized electron gas, with exact small-wave-vector and high-density scaling. Phys Rev 44:B13298-B13307

[15] Alfè D, Kresse G, Gillan MJ (2000) Structure and dynamics of liquid iron under Earth's core conditions. Phys Rev 61:B132-B142

[16] Mao K, Wu Y, Chen LC, Shu JF, Jephcoat AP (1990) Static compression of iron to 300 GPa and Fe0.8Ni0.2 alloy to 260 GPa: implications for composition of the core. J Geophys Res 95:21737-21742

[17] Dewaele A, Loubeyre P, Occelli F, Mezouar M, Dorogokupets PI, Torrent M (2006) Quasihydrostatic equation of state of iron above 2 Mbar. Phys Rev 97:L215504 1-4

[18] Sola E, Brodholt JP, Alfè D (2009) Equation of state of hexagonal closed packed iron under Earth's core conditions from quantum Monte Carlo calculations. Phys Rev 79:B024107 1-6

[19] Wallace DC (1998) Thermodynamics of Crystals. Dover Publications, New York

[20] Stixrude L, Cohen RE (1995) High-pressure elasticity of iron and anisotropy of Earth's inner core. Science 267:1972-1975

[21] Frenkel D, Smit B (1996) Understanding molecular simulation. Academic Press, San Diego

[22] Steinle-Neumann G, Stixrude L, Cohen RE, Gülseren O (2001) Elasticity of iron at the temperature of the Earth's inner core. Nature 413:57-60

[23] Gannarelli C, Alfè D, Gillan MJ (2003) The particle-in-cell model for ab initio thermodynamics: implications for the elastic anisotropy of the Earth's inner core. Phys Earth Planet Int 139:243-253

[24] Gannarelli CMS, Alfè D, Gillan MJ (2005) The axial ratio of hcp iron at the conditions of the Earth's inner core. Phys Earth Planet Inter 152:67-77

[25] Ma Y, Somayazulu M, Shen G, Mao HK, Shu J, Hemley RJ (2004) In situ X-ray diffraction studies of iron to Earth-core conditions. Phys Earth Planet Int 143-144:455-467

[26] Vočadlo L (2007) Ab initio calculations of the elasticity of iron and iron alloys at inner core conditions: evidence for a partially molten inner core? Earth Plan Sci 254:L227-L232

[27] Allen MP, Tildesley DJ (1987) Computer simulation of liquids. Oxford Science Publications, Oxford

[28] de Wijs GA, Kresse G, Gillan MJ (1998) First-order phase transitions by first-principles free-energy calculations: the melting of Al. Phys Rev 57:B8223-B8234

[29] Alfè D, Gillan MJ (1998b) First-principles calculation of transport coefficients. Phys Rev 81:L5161-L5164

[30] Alfè D, Gillan MJ (1998a) First-principles simulations of liquid Fe-S under Earth's core conditions. Phys Rev 58:B8248-B8256

[31] Alfè D (2009a) PHON A program to calculate phonons using the small displacement method. Comput Phys Commun 180:2622-2633. Program available at http://chianti.geol.ucl.ac.uk/∼dario.

[32] Brockhouse BN, Abou-Helal HE, Hallman ED (1967) Lattice vibrations in iron at 296 K. Solid State Commun 5:211-216

[33] Seto M, Yoda Y, Kikuta S, Zhang XW, Ando M (1995) Observation of nuclear resonant scattering accompanied by phonon excitation using synchrotron radiation. Phys Rev 74: L3828-L3831

[34] Sturhahn W, Toellner TS, Alp EE, Zhang X, Ando M, Yoda Y, Kikuta S, Seto M, Kimball CW, Dabrowski B (1995) Phonon density of states measured by inelastic nuclear resonant scattering. Phys Rev 74:L3832-L3835

[35] Mao HK, Xu J, Struzhkin VV, Shu J, Hemley RJ, Sturhahn W, Hu MY, Alp EE, Vočadlo L, Alfè D, Price GD, Gillan MJ, Schwoerer-Böhning M, Häusermann D, Eng P, Shen G, Giefers H, Lübbers R, Wörtmann G (2001) Phonon density of states of iron up to 153 Gigapascals. Science 292: 914-916

[36] Alfè D, Price GD, Gillan MJ (2001) Thermodynamics of hexagonal-close-packed iron under Earth's core conditions Phys Rev 64:B045123 1-16

[37] Watanabe M, Reinhardt WP (1990) Direct dynamical calculation of entropy and free energy by adiabatic switching. Phys. Rev. 65:L3301-L3304

[38] Poirier J-P (1991) Introduction to the physics of the Earth's interior. Cambridge University Press, Cambridge, England.

[39] Alfè D, Gillan MJ, Price GD (2002a) Iron under Earth's core conditions: liquid-state thermodynamics and high-pressure melting curve from ab initio calculations. Phys Rev 65: B165118 1-11

[40] Brown JM, McQueen RG (1986) Phase transitions, Grüneisen parameter and elasticity for shocked iron between 77 GPa and 400 GPa. J Geophys Res 91:7485-7494

[41] Alfè D, Gillan MJ, Price GD (1999) The melting curve of iron at the pressures of the Earth's core from ab initio calculations. Nature 401:462-464

[42] Bukowinski MST (1999) Earth science: taking the core temperature. Nature 401:432-433

[43] Boehler R (1993) Temperatures in the Earth's core from melting-point measurements of iron at high static pressures. Nature 363:534-536

[44] Shen G, Mao HK, Hemley RJ, Duffy TS, Rivers ML (1998) Melting and crystal structure of iron at high pressures and temperatures. Geophys Res 25:L373-L376

[45] Nguyen JH, Holmes NC (2004) Melting of iron at the physical conditions of the Earth's core. Nature 427:339-342

[46] Laio A, Bernard S, Chiarotti GL, Scandolo S, Tosatti E (2000) Physics of Iron at Earth's Core Conditions. Science 287:1027-1030

[47] Belonoshko AB, Ahuja R, Johansson B (2000) Quasi-ab initio molecular dynamic study of Fe melting. Phys Rev 84:L3638-L3641

[48] Alfè D, Price GD, Gillan MJ (2002b) Complementary approaches to the ab initio calculation of melting properties. J Chem Phys 116:6170-6177

[49] Alfè D (2009b) Temperature of the inner-core boundary of the Earth: melting of iron at high pressure from first-principles coexistence simulations. Phys Rev 79:B060101(R) 1-4

[50] Sola E, Alfè D (2009) Melting of iron under Earth's core conditions from diffusion Monte Carlo free energy calculations. Phys Rev 103:L078501 1-4

[51] Kresse G, Furthmuller J (1996). Efficiency of ab-initio total energy calculations for metals and semiconductors using a plane-wave basis set. Comput Mater Sci 6: 15-50. Efficient iterative schemes for ab initio total-energy calculations using a plane-wave basis set. Phys Rev 54:B11169-B11186

[52] Needs RJ, Towler MD, Drummond ND, Lopez Rios P (2007) CASINO version 2.1 User Manual. University of Cambridge, Cambridge

[53] Yoo CS, Holmes NC, Ross M, Webb DJ, Pike C (1993) Shock temperatures and melting of iron at Earth core conditions. Phys Rev 70:L3931-L3934

[54] Williams Q, Jeanloz R, Bass JD, Svendesen B, Ahrens TJ (1987) The melting curve of iron to 250 Gigapascals: a constraint on the temperature at Earth's center. Science 286:181-182

[55] Jephcoat AP, Besedin SP (1996) Temperature measurement and melting determination in the laser-heated diamond-anvil cell. Phil Trans Royal Soc London A 354:1333-1360